New Journal of Physics
The open access journal at the forefront of physics

Deutsche Physikalische Gesellschaft DPG IOP Institute of Physics

PAPER • OPEN ACCESS

On space charge effects in laboratory-based photoemission electron microscopy using compact gas discharge extreme ultraviolet sources

To cite this article: Daniel Wilson *et al* 2020 *New J. Phys.* **22** 103019

View the article online for updates and enhancements.

This content was downloaded from IP address 93.133.168.141 on 18/11/2020 at 19:33

New Journal of Physics
The open access journal at the forefront of physics

Deutsche Physikalische Gesellschaft DPG
IOP Institute of Physics

Published in partnership with: Deutsche Physikalische Gesellschaft and the Institute of Physics

OPEN ACCESS

RECEIVED
1 June 2020

REVISED
13 September 2020

ACCEPTED FOR PUBLICATION
28 September 2020

PUBLISHED
9 October 2020

Original content from this work may be used under the terms of the Creative Commons Attribution 4.0 licence.

Any further distribution of this work must maintain attribution to the author(s) and the title of the work, journal citation and DOI.

PAPER

On space charge effects in laboratory-based photoemission electron microscopy using compact gas discharge extreme ultraviolet sources

Daniel Wilson[1,2,3,*], **Christoph Schmitz**[1,2], **Denis Rudolf**[1,2], **Carsten Wiemann**[1,2], **Claus M Schneider**[1,2] **and Larissa Juschkin**[1,2,3]

[1] Forschungszentrum Jülich, Peter Grünberg Institut, 52425 Jülich, Germany
[2] Jülich-Aachen Research Alliance (JARA), Fundamentals of Future Information Technology, 52425 Jülich, Germany
[3] RWTH Aachen University, Experimental Physics of EUV, 52074 Aachen, Germany
[*] Author to whom any correspondence should be addressed.

E-mail: daniel.wilson@rwth-aachen.de

Keywords: space charge effects, laboratory-based, photoemission electron microscopy, gas discharge EUV source, structural properties of surfaces, improve spatial- and energy-resolution, XPS

Abstract

The analysis of electronic and structural properties of surfaces has been greatly advanced by photoemission electron microscopy and spectroscopy techniques. To further improve lateral and energy resolution of the instruments, it is necessary to optimize parameters of the radiation sources employed for photoemission studies (e.g. photon flux, pulse duration, spot size etc). We studied space charge effects observed in an energy-filtering photoemission electron microscope operated with a compact laboratory-scale gas-discharge extreme ultraviolet light source. In this system, we found limits of spatial- and energy-resolution controlled by the source radiation parameters. The pulse repetition rate can be varied in the kHz range and the duration of the EUV emission was measured to be several tens of nanoseconds long, and thereby very different from the standard synchrotron sources typically used for similar experiments. The spatial resolution could be improved by a factor of 5, but only on the expense of the photon density per pulse, which had to be decreased by a factor of 17 in order to reduce the image blur due to space charge effects. Furthermore, we found broadening of the x-ray photoelectron spectroscopy peaks for high photon fluxes. We have also performed a *n*-body Monte Carlo simulation to evaluate the difference between core-level photoelectrons and secondary electrons with respect to space charge.

Photoemission electron microscopy (PEEM) and spectroscopy (PES) are well established and commonly used methods to study and characterize electronic and structural properties of solids, molecules and thin films with high energy or/and spatial resolution [1]. Spectroscopic microscopy became feasible with energy-filtering instruments (EF-PEEM) and has contributed substantially to the understanding of the electronic structure and chemical states in condensed matter. To further extend the capabilities of this technique in a laboratory environment, and to improve the instrument's lateral and energy resolution, substantial efforts have been invested especially in the development of new light sources optimized for the EF-PEEM. One particular challenge for lateral and energy resolution in photoelectron microscopy and spectroscopy is overcoming parasitic space charge effects, most prominent when EF-PEEM operates with x-ray free electron laser (XFEL) or fs-laser high harmonic generation light sources. The space charge effects are associated with the ultra-short duration of the radiation pulses resulting in high densities of photoelectrons [2–6].

The space charge effect is a phenomenon originating from the collective Coulomb interaction (repulsion) of free charges in space or mirror charges on a metallic sample surface, limiting the performance of charged particle optics, in particular, in the (energy-filtered) photoelectron emission microscopes [4–9], where crossovers of the electron trajectories may lead to high charge densities. For PEEM and PES, space-charge results in a deterioration of the spatial resolution and also in a broadening

© 2020 The Author(s). Published by IOP Publishing Ltd on behalf of the Institute of Physics and Deutsche Physikalische Gesellschaft

and a shift of the photoemission peaks in the energy spectrum. Space charge effects in electron beams have been studied as early as in 1954 by Boersch [10], resulting in the understanding of a broadening and more symmetric energy distribution of the electrons with increased beam current. Another effect, called the trajectory displacement effect, limits the sharpness of the PEEM images and was first described by Loeffler [11]. A comprehensive theoretical description of these and also other effects in charged particle beams can be found in [12]. These initial studies on the behavior of electrons provided a hint in explaining the present observations in our experiments, namely an increase in the measured width of the photoemission peaks and a degradation of lateral resolution.

In our previous article on the combination of a state-of-the-art PEEM and a gas discharge extreme ultraviolet (EUV) source, we recognized a difference in lateral resolution when using the EUV gas discharge light source as compared to the 4.9 eV photon energy mercury lamp source [13]. The observation of degraded lateral resolution and increased width of the core-level peaks is studied now in more detail.

In this paper, we present the dependence of the lateral and energetic resolution on the photon flux obtained from systematic measurements with an (EF-PEEM, Focus NanoESCA [13–17]) and the high power gas discharge EUV source [18–21] at the photon energy of 71.7 eV or 17.3 nm wavelength. Our sample was a bismuth telluride thin film (30 nm) on a Si(111) substrate. The results support the interpretation that the observed changes in performance can be attributed to spatial blurring induced by space charge effects. Furthermore, we simulated the trajectories of electrons emerging from the sample and traveling towards the microscope entrance in a n-body simulation to investigate the impact of electron emission rate and spot size for two cases: secondary electrons are compared to core level electrons with a higher initial kinetic energy. This study suggests that even outside of the microscope there is a distortion of the electron trajectories due to interaction between electrons on their way to the microscope. This effect may be strong, if the illuminated area on the sample is significantly larger than the field of view of the microscope, which is the case here.

The article is structured as follows: first, an overview of the experimental setup including a short description of the EUV source operation principle is given in section 1. In section 2, the results of measurements of the lateral blurring and broadening of spectral peaks are provided. In section 3, the experimental results are compared to other published data as well as simulations and discussed. The findings are summarized in section 4.

1. Experimental setup

The discharge-produced plasma EUV source [(1) in figure 1] consists of a high voltage capacitor array storing the electrical energy E_{el}, which is connected to an electrode system filled with the working gas. The geometry of the electrode system consisting of a cathode, an anode and trigger pins [21] is configured to match the pseudo-spark discharge region of the Paschen curve at operating gas pressures of several Pa and breakdown voltages of a few kilovolts [20]. During the capacitors charging, the trigger pins are set to a positive voltage of a few hundreds volts with respect to the cathode potential to remove negative free charge carriers and therefore to impede the breakdown. When charging of the capacitors is completed, the trigger pins [18] are set to the cathode voltage, allowing electrons to acquire enough energy and ionize the fuel gas creating more and more free electrons and thus, initiating an avalanche breakdown. This discharge bridges the electrodes, allowing for currents of several tens of kiloamperes to heat the plasma and compress the plasma column by the self-induced strong magnetic field of the current via Lorentz force, commonly referred to as the pinch-effect. Finally, the plasma electron density and temperature reach their maximum of about $n_e \approx 1 \times 10^{18}$ cm^{-3} and $T_e \approx 20$ eV$/k_B$, respectively. These plasma conditions are optimal for efficient generation of radiation at 17.3 nm wavelength in oxygen plasma. The optimal conditions may be different for other gases, e.g. for xenon (10.9 nm central wavelength). In general, such highly ionised hot and dense plasma emits characteristic radiation of ion species in quite broad EUV spectral range and allows for fine spectral tuning. Increasing the amount of electrical energy in the discharge increases the EUV photon emission. In contrast to other EUV sources for photoelectron microscopy and spectroscopy, the duration of the EUV emission is in the order of tens of nanoseconds with a kilohertz repetition rate. Per pulse, several millijoules of EUV energy are emitted into a solid angle of 2πsr, distributed over multiple spectral emission lines.

Further, an aperture [(2) in figure 1] limits the solid angle and defines the numerical aperture of the imaging monochromator where the EUV light is monochromatized and transferred to the sample by a set of narrow bandwidth ($\Delta\lambda < 0.3$ nm) Al/Mo-based Bragg mirrors consisting of a flat (3) and a concave mirror (4) (radius $R = 1$ m). The Bragg mirrors are optimized to select only the spectral lines emitted by Li-like O^{5+} ions around $h\nu = 71.7$ eV photon energy ($1s^2 3d$ to $1s^2 2p$ transition) and focus the light onto

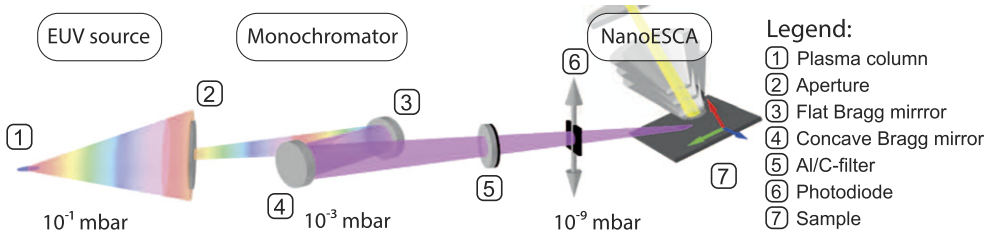

Figure 1. Sketch of the experimental setup. A gas-discharge source emits an EUV spectrum consisting of several separated emission lines (1). An aperture (2) limits the solid angle and defines the numerical aperture of the imaging monochromator which consists of two narrow bandwidth Bragg mirrors, a flat one (3) and a concave one ($R = 1$ m) (4) to focus the light onto the sample (7). Behind the monochromator, the light is spectrally filtered with only emission lines at 17.3 nm wavelength ($h\nu = 71.7$ eV) remaining. To block visible light and maintain the UHV conditions of 10^{-9} mbar inside the Focus NanoESCA, a EUV transparent metal filter (5) is used. A calibrated photodiode (6) mounted on a linear manipulator is used to measure the energy per pulse behind the optical system. The EUV photons create photoelectrons at the sample surface (7) which are energy-filtered and imaged (EF-PEEM) onto a 2D detector behind the two hemispherical analyzers (not shown, see [13]). Reprinted from [13], with the permission of AIP Publishing.

the sample (7) at 65° angle of incidence to the normal. To maintain the required UHV conditions of 10^{-9} mbar in the PEEM, while having plasma operation conditions (10^{-1} mbar) in the discharge region of the source, a differential pumping scheme and a thin, almost EUV transparent Al(151.4 nm)/C(28.1 nm) metal filter (5) are used for vacuum separation and to block visible light.

To measure the energy per pulse, a calibrated AXUV100 photodiode on a mechanical manipulator (6) was put into the beam path before the Focus NanoESCA. Additionally, Zemax [22] ray tracing simulations of the beam path are performed to account for shadowing effects and spherical aberrations of the monochromator and to determine the correct illumination spot size at the sample. Further, the solid angle captured by the optical system and the photodiode is also extracted to determine the energy per pulse emitted by the source regardless of the optical system for further calculations. The duration of EUV emission t_e for the $h\nu = 71.7$ eV emission line of oxygen was measured to $t_e = 63.3$ ns $\pm$ 11.2 ns at full width at half maximum (FWHM). The source emits an average energy per pulse E_{pp} of 1.16 ± 0.16 mJ/2πsr for the strong emission line at 17.29 nm combined with its weaker satellite, with 2.5 kV voltage applied to the capacitor bank of 0.996 μF and 100 sccm oxygen gas flow through the electrode system.

2. Space charge effects

2.1. Lateral broadening

Due to a visible deterioration of lateral resolution for images taken with the pulsed EUV gas discharge source compared to images taken with the conventional HG-lamp [13], we performed a systematic study using the Focus NanoESCA and our EUV gas discharge source. We define lateral resolution as the distance from 10% to 90% rise of the maximum intensity at a sharp edge. Thus, an increase in this distance is related to a less detailed picture.

In order to identify if the degradation in resolution originates from space charge effects, we took several images of a structure (scratch) in a Bi_2Te_3 thin film close to the work function cut-off at photoelectron kinetic energy of 4.2 eV. This mode of operation is also called secondary electron imaging. Figure 2(a)) shows an image of the scratch acquired with the standard mercury discharge lamp for reference. When switching to EUV radiation, we observed a substantial blurring of the image which was dependent on the energy per pulse of the EUV source. This effect is presented in figure 2(b) where one can see the same area of the sample as shown in (a), but illuminated with the EUV source (inset in (b)). The red stripe in the insert shows where the line profiles were evaluated. We find an increased broadening of the line profiles with the increase of the number of electrons per pulse contributing to the images. In order to convert the applied voltage to the number of emitted photons per area and pulse, we used a previously measured source emission calibration curve to translate the applied voltage U_s of the EUV source to energy per pulse. The results are shown in figure 3 exhibiting an increasing image blur for increasing number of photons per area and pulse (x-axis). Space charge effects should highly depend on the peak fluence at the sample, given in photons or energy per area and time. With increasing energy per pulse (horizontal), blurring of the image becomes more and more pronounced, while with increasing repetition rate (vertical), only the signal-to-noise ratio is enhanced.

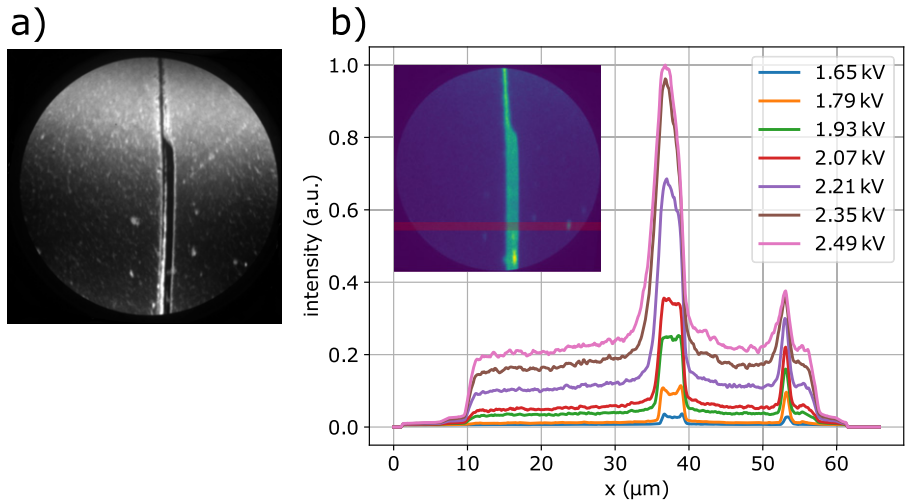

Figure 2. (a) Image of the scratch acquired with the standard mercury discharge lamp as a reference to images acquired with the EUV-lamp. (b) Exemplary plot of line profiles in dependence of charging voltage U_s of the EUV source which directly impacts the number of emitted photons. With increasing voltage and thereby number of photons per pulse, we find an increased broadening of the line profiles which are averaged over the red area shown in the inset. This gradual worsening of resolution is attributed to space charge effects. The nonlinear response of the intensity to charging voltage U_s is expected.

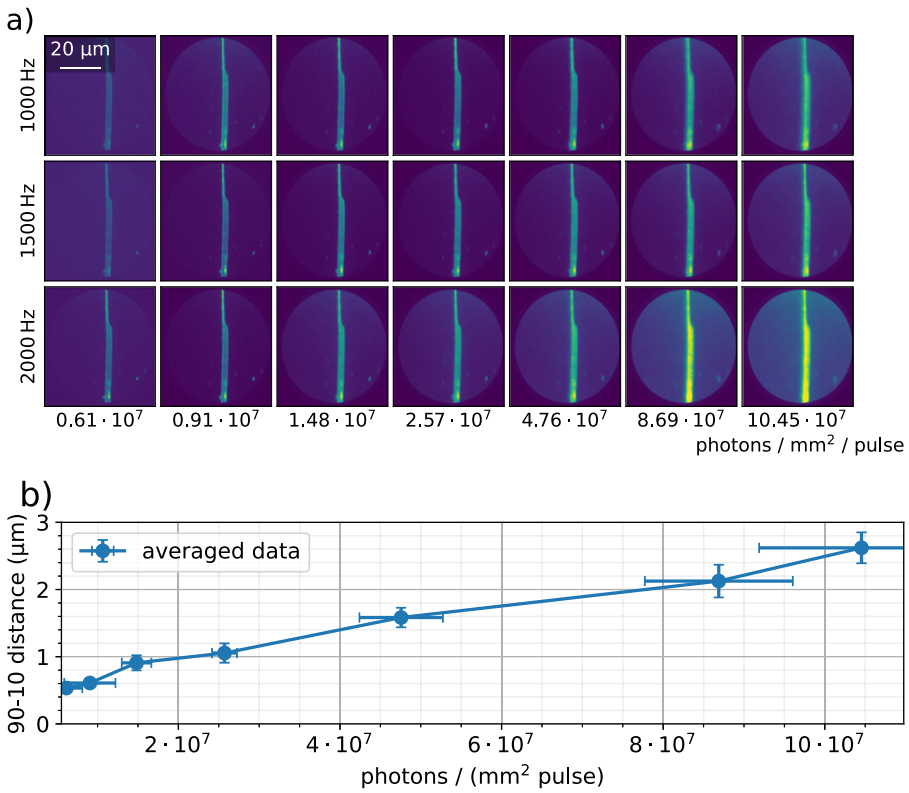

Figure 3. (a) Photoelectron image matrix close to the work function cut-off of the thin film Bi_2Te_3 sample. The greenish to yellow region corresponds to a scratch in the thin film exhibiting lower photoemission signals of the Te 4d and Bi 5d peaks and higher intensity close to the work function cut-off. Images have been acquired for different photon fluxes (0.61×10^7 photons/(mm^2 · pulse) − 1.05×10^8 photons/(mm^2 · pulse), horizontal) and different repetition rates (1–2 kHz, vertical) of the EUV source. All images were acquired with same PEEM settings: field of view of 55 μm, integration time of 20 s and an electron kinetic energy $E_{kin} = 4.2$ eV. (b) Lateral resolution was averaged over a few regions on the sample and over three repetition rates of the EUV source. The 10%–90% distance increases as expected with increasing photon density per pulse, but is independent of the repetition rate. Increasing repetition rate is beneficial as the signal to noise ratio increases, while keeping the integration time constant. Error-bars indicate the spread of data in the measurements at different source repetition rates, while measurement positions within the image are kept constant for all images.

The contrast originates from the sample's morphology, which may lead to a distortion of the electric field at the sample affecting the image [7]. Lens settings for a field of view of 55 μm and an acquisition time

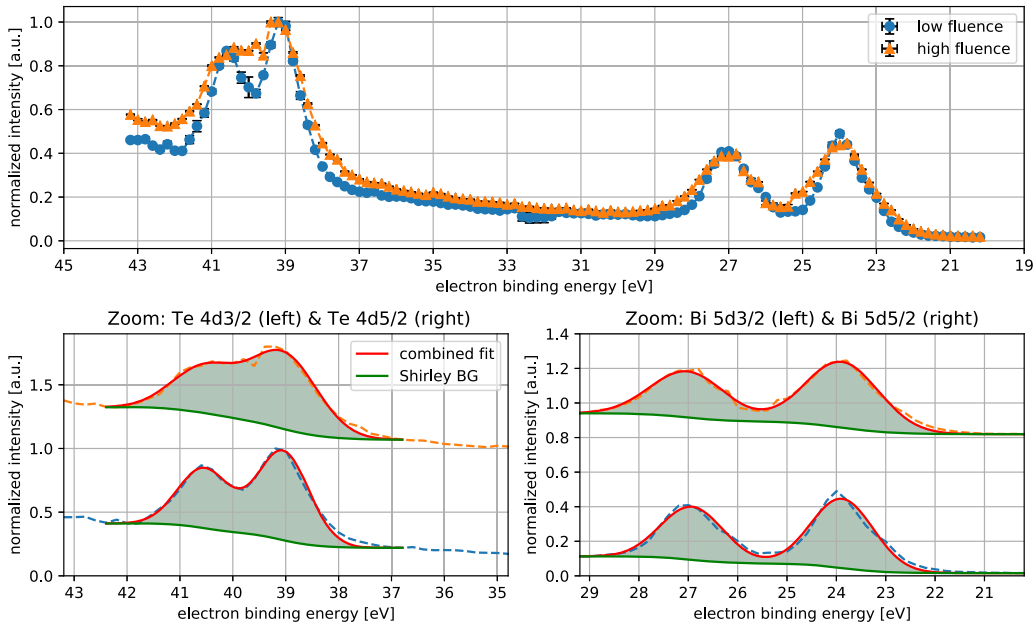

Figure 4. (a) Normalized photoemission spectra of a Bi_2Te_3 thin film sample for high and low photon fluence on the sample. Each datapoint represents the summed intensity of an energy-filtered PEEM image at a certain binding energy. Integration time was 1 s per image with 200 meV steps and a EUV source repetition rate of 2 kHz for both measurements. Triangles represent measurement with high fluence (1.05×10^8 photons/(mm^2 · pulse) or 1.74×10^4 W m^{-2}) and circles with low fluence (0.91×10^7 photons/(mm^2 · pulse) or 1.75×10^3 W m^{-2}). (b) (Left) Fit of each individual Te 4d peak (green area) as well as the combined peak (red line) including the Shirley background (green line) for both fluence regimes. Curves have been shifted for better visibility. For high fluence (upper curve), the seperation between the Te 4d3/2 and Te 4d5/2 is less pronounced than for the bottom measurement with lowered fluence. (b) (Right) Similar fit to the Bi 5d peaks showing the same behaviour as for the Te 4d binding energy region. All fit parameters are summarized in table 1. A systematic broadening of the peaks is apparent for the high fluence measurement originating from space charge effects.

of 20 s are the same for each image. To quantify the results, we performed resolution measurements by taking line scans at different positions across the sharp edge of the scratch and averaging the results. The averaging was furthermore performed for three measurements sets each taken at a different repetition rate of the EUV source, 1.0 kHz, 1.5 kHz and 2.0 kHz. The spatial range between 10% and 90% values of the intensity is shown in figure 3.

The resolution degrades with increasing number of photons per pulse for all repetition rates. The error bars indicate the spread between three measurement series performed at different repetition rates and therefore slightly different source operation conditions. These can not be attributed directly to space charge effects, but to the fact that the gas flow in the EUV source needs to be adjusted for proper operation if the repetition rate is changed, and is also dependent on the electrodes life-time. Since the numbers of photons at the sample are interpolated from a previously measured calibration curve with the charging voltage of the EUV source as input, differences may arise if the pressure conditions are not exactly the same. In order to address this uncertainty, we used a defined area of the images with homogeneous intensity to determine the spread between intensity counts at different repetition rates of the EUV source and scaled this variation to the number of photons per area and pulse, shown as the x-error in figure 3(b). Nevertheless, the trend in degradation of resolution is clearly visible and can be ascribed to the increasing number of photons per area and pulse.

2.2. Energetic broadening

To quantify a change in the energetic resolution in dependence of the peak fluence, two scans in energy-filtered PEEM mode with 200 meV step size and pass energy $E_{\text{pass}} = 100$ V have been performed and are shown in the top part of figure 4. For each of the two curves, five consecutive scans were averaged with standard deviation indicated by the error bars. The blue (circles) curve was measured with a peak fluence of 1.75×10^3 W m^{-2} and the orange curve (triangles) with 1.74×10^4 W m^{-2}, differing by one order of magnitude. The spin–orbit splitting of Te 4d3/2 and Te 4d5/2 is more pronounced for the low peak intensity measurement. Bottom part of figure 4 shows a zoom to the Te 4d and Bi 5d peaks with two fitted Gaussians on top of a Shirley background [23]. Fitting parameters are summarized in table 1 exhibiting a systematic broadening of the peaks for high fluence, more pronounced for the Te peaks which may be related to the lower kinetic energy of the electrons. For very high peak fluences and ultra-short pulse

Table 1. Width σ and position μ of fitted Gaussians for different binding energy peaks of Te 4d and Bi 5d for measurements with high and low fluence in comparison. The width of the peaks of the same element was set equal while fitting, since we only expect a negligible difference in width for spin–orbit split photoemission peaks. Most notable is the increased width for high fluence compared to low fluence for both elements, a result of the space charge effects.

Measurement	Te 4d3/2	Te 4d5/2	Bi 5d3/2	Bi 5d5/2
Low fluence: 1.75×10^3 W m^{-2}	$\sigma = 489$ meV		$\sigma = 630$ meV	
	$\mu_0 = 40.55$ eV	$\mu_1 = 39.05$ eV	$\mu_0 = 26.92$ eV	$\mu_1 = 23.88$ eV
High fluence: 1.74×10^4 W m^{-2}	$\sigma = 625$ meV		$\sigma = 747$ meV	
	$\mu_0 = 40.51$ eV	$\mu_1 = 39.03$ eV	$\mu_0 = 27.02$ eV	$\mu_1 = 23.88$ eV

durations of XFEL sources, this phenomenon has been observed before. While for measurements at XFELs with extreme fluences, shifts in binding energy due to space charge occur in negative direction [6, 8], no significant shift in binding energy was observed in our measurements. The average difference of peak positions for low- and high-fluence measurements is 9 ± 49 meV for the four peaks and has the same magnitude as the error given by the fit algorithm related to the energy stepping of 200 meV.

3. Discussion and comparison to related works

Comparing space charge effects observed in different setups is challenging due to the considerable differences in parameters of the experiments. They differ in photon sources, e.g. photon energy, pulse duration, photon fluence at samples and spot sizes. Also, samples are different, exhibiting different photoionization cross-sections and thus the amount of electrons emitted for the number of absorbed photons differs. Furthermore, microscopes differ in operation principle, number of crossings of electron trajectories, electron speeds at these crossings, and microscope settings. Our setup (figure 1) was designed to have a low electron flux to avoid any space charge effects, but these effects are still evident even though the source can be operated at the low energy per pulse mode. We compare photon and photoelectron related parameters based on our and others results in a similar way as in [9].

To estimate the emitted number of secondary electrons we took measured values for the secondary electron quantum yield from [24] where the insulator and semiconductor photocathodes exhibit a considerably higher secondary electron yield than the metallic Au and Al photocathodes. We accounted for this by approximating the electron yield from 1 for non-metallic to 0.1 for metallic samples in the EUV for the following discussion. Furthermore, we included the reflectivity of the samples [25] into the estimation of the number of photons being absorbed by the sample, since angle of incidence also differs between the experiments. We then calculated the electron emission rate [e$^-$ fs^{-1}] and the electron flux [e$^-$ fs^{-1} μm^{-2}]. The duty cycle is defined as the repetition rate times pulse duration, thus a duty cycle of unity represents continuous wave light sources. The resulting parameters are summarized in table 2.

The selected experiments where space charge effects occurred differ in most of their parameters, e.g. by orders of magnitude in the electron rate and flux. For [9], the resolution becomes worse than 50 nm for 3.6×10^{-3} e$^-$ (fs^{-1} μm^{-2}) for core-level electrons and the same applies to secondary electrons in greater extent due to their lower velocity. In our measurements, the electron flux is orders of magnitude lower, but due to the rather large spot size the total number of electrons ejected from the sample per femtosecond (electron rate) is of the same order of magnitude. The duty cycle of the light source is connected to the efficiency regarding PEEM experiments. A low duty cycle leads to increased time to acquire an image or to severe space charge induced limitations because of the increased number of electrons in time. Considering [2, 26] and our measurements, it is plausible that the spot size should be adjusted in order not to exceed the field of view of the microscope by far. All electrons emitted from the sample contribute to space charge effects at the sample, but only a small part contributes to the image. Commonly, this is achieved by introducing a field aperture to minimize electron rate inside the microscope so that only the electrons contributing to the image enter the system, which results in an improvement of the lateral resolution [7]. Nevertheless, the results of Zhou *et al* [26] and our measurements indicate that the large spot size intensifies space charge problems, e.g. by limiting the possible resolution to 100 nm or more. Schmidt *et al* [7] concludes that for their optimized XPEEM, the resolution of 18 nm was limited by space charge effects, which may have occurred in the electron path up to the field aperture. These findings indicate that besides the reported theoretical and measured threshold value for electron flux of about 2 e$^-$/(μm^2 pulse) [4], also the total number of electrons emitted from a single light pulse is important. To further study this problem

Table 2. Comparison of different experiments with observed space charge phenomena.

	This work [NanoESCA]	Locatelli *et al* [9] [SPELEEM III]	Zhuo *et al* [26] [Scienta 2002]	Buckanie *et al* [2] [SPELEEM III]	Schmidt *et al* [7] [SMART microscope]
Photon source	Gas discharge source	Undulator	Undulator	fs laser	Undulator
Photon energy	71.8 eV	182 eV	35 eV	6.2 eV	200 eV
Pulse duration	63.3 ± 11.2 ns	42 ps	60 ps	140 fs	40 ps
Repetition rate	2 kHz	500×10^3 kHz	500×10^3 kHz	250 kHz	500×10^3 kHz
Spot size	4×1.05 mm^2	3×25 μm^2	430×300 μm^2	400×200 μm^2	10×4 μm^2
Photon rate [photons s^{-1}]	8.71×10^{11}	6×10^{13}	1×10^{13}	5.03×10^{12}	8×10^{11}
Reflectivity	5.5×10^{-2}	4.5×10^{-2}	3.8×10^{-1}	NA	5×10^{-3}
Photons absorbed [photons/pulse]	4.11×10^8	4.95×10^7	1.24×10^4	2.01×10^7	1.59×10^3
Electron yield [e$^-$/photon]	1	0.1	0.1	1×10^{-3}	0.1
Electron rate [e$^-$ fs^{-1}]	6.49	2.7×10^{-1}	2.1×10^{-2}	1.4×10^2	4×10^{-3}
Electron flux [e$^-$ fs^{-1} μm^{-2}]	1.6×10^{-6}	3.6×10^{-3}	1×10^{-7}	1.8×10^{-3}	1×10^{-4}
Duty cycle	1.27×10^{-4}	2.1×10^{-2}	3×10^{-2}	3.5×10^{-8}	2×10^{-2}
Spatial resolution	0.5 μm–2.5 μm	35 nm–180 nm	No imaging	Not given	18 nm–500 nm

we posed the question about how electron displacement caused by space charge varies close to the sample and how it depends on the spot size for a constant electron flux.

The study's focus is put on the interactions of the electrons on their way from the sample to the entrance of the microscope. In our experiment, the illumination spot size was much larger than the field-of-view of the microscope and the resolution we could reach was worse than in other experiments, or for the continuous HG-lamp, thus we suspected strong impact on the lateral resolution from electrons that do not contribute to the image in the microscope. Generally, the situation inside the microscope is much more difficult to describe. Despite the inherent differences of different microscopes in their design, space charge effects inside the microscope depend on where the electrons are filtered by energy, the corresponding slit width, size of the contrast aperture and the point where electrons from outside of the field of view are filtered. In our study, we performed an n-body Monte Carlo simulation of electrons, with a Poisson distribution in time domain during a pulse of Gaussian temporal shape. Spatially, the illumination has been set uniform over a chessboard-like structure, with the electron initial momentum perpendicular to the sample surface. Image charge is not taken into account, since it creates no displacement in the sample plane. An electric field of $E_z = 24$ kV cm^{-1} accelerates the simulated electrons in z-direction. At each time step, in this study set to 20 fs, the position of electrons is advanced in time and the acceleration by other particles in x, y and z-direction is calculated. We define the displacement as the average absolute difference between the lateral position at $t_0 = 0$ and the position at a certain time t_1, which is set to $t_1 = 30$ ps for simulations shown in figure 5, which is the approximate time when the core level electrons with $E_{\mathrm{kin}} = 147$ eV reach a position around 0.39 mm above the sample and the secondary electrons with $E_{\mathrm{kin}} = 4$ eV around 0.22 mm. This emphasizes that there is an inherent difference with respect to the electron kinetic energy and space charge effect, which cannot be attributed to the longer time of flight. The reason is that the electrons do not emerge from the sample at the same time, and the electric field exerts a force on the electrons, which results in a longer effective 'dwelling' time in the proximity of the sample for slower electrons. Consequently, electrons that have lower initial kinetic energy have a higher probability to have other electrons in their vicinity close to the sample, whereas core-level electrons will increase their distance from new emerging electrons much faster. In the case that all electrons are evaluated at the same z-distance, the orange curve for the secondary electrons in figure 5 indicates the range of displacement from 11.2 nm to 58 nm, and shows exactly the same behavior. It is important to note that the core-level and secondary electrons curves are obtained from separate simulations, thus there is no interaction between the two groups of photo-electrons. Generally, a simulation that considers both types of electrons is possible to implement, but would need additional assumptions on the ratio of the number of secondary to core-level electrons and thus makes the results sample dependent. With one electron only at a time, there would be no displacement since only the z-component of the electric field is taken into account which simplifies the analysis of the data.

The electron flux was set to 1.27×10^{-4} e$^-$ (fs^{-1} μm^{-2}) which corresponds to 400 e$^-$ per pulse from a 75 μm^2 area with 42 ps FWHM light pulses for both cases, but increases to several thousand electrons active at the same time with increasing area as occurred in figure 5. These parameters describe the situation of [9]. The reason for choosing settings that are different from our own experiment is that the absolute number of electrons emitted from the sample is too high to simulate n-body interactions in a reasonable amount of time.

For small spot sizes, the resulting displacement shows a non linear behavior which progresses linearly above roughly 700 μm^2 spot size. For lower electron flux, e.g. values close to our measurements, the

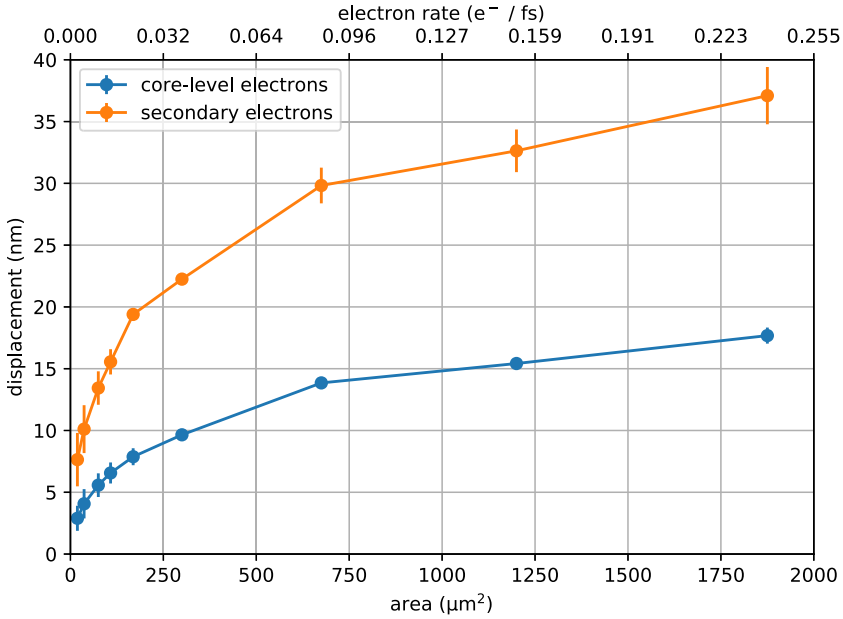

Figure 5. Simulated average displacement from original position at sample for electrons with kinetic energy $E_{kin} = 4$ eV (secondaries) and electrons with high $E_{kin} = 147$ eV (core-level) due to Coulomb repulsion. The electron flux was set to 1.27×10^{-4} e$^-$ (fs^{-1} μm^{-2}) which corresponds to $\approx$400 e$^-$ per pulse from a 75 μm^2 area with 42 ps FWHM light pulses. Values are given after 30 ps flight time corresponding to 387 μm and 220 μm above the sample for fast and slow electrons, respectively. Clearly visible is the nonlinear trend for small spot sizes which becomes linear after roughly 700 μm^2 spot size.

displacement is two or three orders of magnitude lower than the experimentally observed resolution of several hundred nm, indicating also the importance of the total electron rate which is significantly higher in our experiment compared to others (table 2). Since the electron crossings in the microscope are not part of the simulation, it indicates that a significant contribution to the overall displacement by space charge effects may arise from there.

We conclude that the overall number of electrons at the trajectory crossings inside the microscope greatly affects the resolution because of the lowered distance between the electrons. Usage of a small contrast aperture limits the number of electrons at crossings that remain behind the aperture, and thus improves resolution. However our simulation shows that space charge also affects the electrons before they enter the microscope and that the illumination spot size plays an important role and should match the field-of-view of the microscope.

Another effect of a smaller contrast aperture is the reduction of angle dependent aberrations, thus improving the resolution. Nevertheless, the number of electrons behind the contrast aperture is dependent on the electron emission rate, which is relatively high in our case compared to other measurements (table 2), although electron flux is at least two orders of magnitude lower. On the contrary for small illumination spots, e.g. as in [7, 9], with sufficient intensity, our n-body simulation shows that for electron fluxes of 1.27×10^{-4} e$^-$ (fs^{-1} μm^{-2}) at the sample, the electrons will gain an impulse in space before any crossing, leading to a symmetric displacement around the initial position at the sample. For small spot sizes, the electron flux becomes important even if the overall electron rate is small (figure 5).

4. Conclusion

We performed spectromicroscopy with a laboratory-based gas discharge EUV light source and a Focus NanoESCA on a Bi_2Te_3 sample with a photon energy of 71.8 eV and observed space charge effects limiting the resolution. Characteristics of the used EUV gas discharge light source differ strongly compared to synchrotrons and other kinds of EUV light sources. The repetition rate can be varied in the kHz range and the EUV emission pulse duration was measured to be 63.3 ± 11.2 ns. Depending on the discharge electrical energy E_{el}, the emitted number of photons or energy per pulse E_{pp} was varied by one order of magnitude which allows adjusting the photon rate at the sample to reduce space charge effects. We observed space charge effects on a thin film Bi_2Te_3 sample, limiting the resolution of our measurements even though the electron flux in e$^-$ (fs^{-1} μm^{-2}) was about two orders of magnitude lower than for other experiments where space charge effects were also the limiting factor. Knife-edge intensity rise extent (10%–90%) increased by a factor of 5 when the peak intensity in the pulse has been risen by a factor of 17. This illustrates the

degradation of resolution with the increase of the number of photons per pulse per mm^2. In comparison to other experiments studying space charge effects, the number of emitted electrons per area and pulse is much lower in our case, nevertheless, we could also observe the broadening of the photoemission peaks due to the space charge. In our *n*-body Monte Carlo simulation we demonstrated that for small illumination spots and low electron emission rates found in other publications, the resolution can still be limited by Coulomb interaction of the electrons in the proximity of the sample and not only inside the microscope. Additionally, core-level electrons are less deflected due to their higher take-off velocity. For our measurements, the high electron emission rate from an illumination spot that exceeded the field of view of the microscope by far, was limiting our spatial resolution.

Acknowledgments

This work was realized by cooperation activities in the frame of the Jülich Aachen Research Alliance for Fundamentals of Future Information Technology (JARA-FIT). LJ acknowledges financial support from the Helmholtz Association for a Helmholtz Professorship as a part of the Initiative and Networking Fund.

References

[1] Reinert F and Hüfner S 2005 Photoemission spectroscopy–from early days to recent applications *New J. Phys.* **7** 97
[2] Buckanie N M, Göhre J, Zhou P, von der Linde D, Horn-von Hoegen M and Meyer zu Heringdorf F-J 2009 Space charge effects in photoemission electron microscopy using amplified femtosecond laser pulses *J. Phys.: Condens. Matter* **21** 314003
[3] Oloff L-P, Hanff K, Stange A, Rohde G, Diekmann F, Bauer M and Rossnagel K 2016 Pump laser-induced space-charge effects in HHG-driven time- and angle-resolved photoelectron spectroscopy *J. Appl. Phys.* **119** 225106
[4] Mikkelsen A *et al* 2009 Photoemission electron microscopy using extreme ultraviolet attosecond pulse trains *Rev. Sci. Instrum.* **80** 123703
[5] Chew S H *et al* 2012 Erratum: "Vertically coupled photonic molecule laser" [Appl. Phys. Lett. 100, 041103 (2012)] *Appl. Phys. Lett.* **100** 089903
[6] Schönhense G 2015 Correction of the deterministic part of space-charge interaction in momentum microscopy of charged particles *Ultramicroscopy* **159** 488–96
[7] Schmidt T, Sala A, Marchetto H, Umbach E and Freund H-J 2013 First experimental proof for aberration correction in XPEEM: resolution, transmission enhancement, and limitation by space charge effects *Ultramicroscopy* **126** 23–32
[8] Pietzsch A *et al* 2008 Towards time resolved core level photoelectron spectroscopy with femtosecond x-ray free-electron lasers *New J. Phys.* **10** 033004
[9] Locatelli A, Menteş T O, Niño M Á and Bauer E 2011 Image blur and energy broadening effects in XPEEM *Ultramicroscopy* **111** 1447–54
[10] Boersch H 1954 Experimentelle Bestimmung der Energieverteilung in thermisch ausgelösten Elektronenstrahlen *Z. Phys.* **139** 115–46
[11] Loeffler K H 1964 *PhD Thesis* University of Berlin
[12] Jansen G 1990 *Coulomb Interactions in Particle Beams* (*Advances in Electronics and Electron Physics: Supplement*) (New York: Academic)
[13] Schmitz C *et al* 2016 Compact extreme ultraviolet source for laboratory-based photoemission spectromicroscopy *Appl. Phys. Lett.* **108** 234101
[14] Escher M 2005 Nanoelectron spectroscopy for chemical analysis: a novel energy filter for imaging x-ray photoemission spectroscopy *J. Phys.: Condens. Matter* **17** S1329
[15] Weber N B, Escher M, Merkel M, Oelsner A and Schönhense G 2008 Energy- and time-resolved microscopy using PEEM: recent developments and state-of-the-art *J. Phys.: Conf. Ser.* **100** 072031
[16] Wiemann C, Patt M, Cramm S, Escher M, Merkel M, Gloskovskii A, Thiess S, Drube W and Schneider C M 2012 Probing buried layers by photoelectron spectromicroscopy with hard x-ray excitation *Appl. Phys. Lett.* **100** 223106
[17] Escher M, Winkler K, Renault O and Barrett N 2010 Applications of high lateral and energy resolution imaging XPS with a double hemispherical analyser based spectromicroscope *J. Electron Spectrosc. Relat. Phenom.* **178–179** 303–16
[18] Pankert J *et al* 2002 Physical properties of the HCT EUV source https://doi.org/10.1117/12.472271
[19] Pankert J *et al* 2003 Physical properties of the HCT EUV source https://doi.org/10.1117/12.483611
[20] Bergmann K, Vieker J and von Wezyk A 2016 Investigations on the emission in the extreme ultraviolet of a pseudospark based discharge light source *J. Appl. Phys.* **120** 143302
[21] Vieker J and Bergmann K 2017 Influence of the electrode wear on the EUV generation of a discharge based extreme ultraviolet light source *J. Phys. D: Appl. Phys.* **50** 345601
[22] ZEMAX 2005 Optical design software ZEMAX
[23] Shirley D A 1972 High-resolution x-ray photoemission spectrum of the valence bands of gold *Phys. Rev.* B **5** 4709–14
[24] Henke B L, Knauer J P and Premaratne K 1981 The characterization of x-ray photocathodes in the 0.1–10 keV photon energy region *J. Appl. Phys.* **52** 1509–20
[25] Henke B L, Gullikson E M and Davis J C 1993 X-Ray interactions: photoabsorption, scattering, transmission, and reflection at $E = 50$-30,000 eV, $Z = 1$-92 *At. Data Nucl. Data Tables* **54** 181–342
[26] Zhou X J, Wannberg B, Yang W L, Brouet V, Sun Z, Douglas J F, Dessau D, Hussain Z and Shen Z-X 2005 Space charge effect and mirror charge effect in photoemission spectroscopy *J. Electron Spectrosc. Relat. Phenom.* **142** 27–38